Climate Dynamics (2020) 54:2029–2039
https://doi.org/10.1007/s00382-019-05101-8

Effect of vertical moist static energy advection on MJO eastward propagation: sensitivity to analysis domain

Lu Wang[1,2] · **Tim Li**[1,3]

Received: 13 July 2019 / Accepted: 21 December 2019 / Published online: 20 January 2020

Abstract

Previous studies have shown great uncertainty in assessing the effect of vertical moist static energy (MSE) advection term to the zonal asymmetry of MSE tendency. This study addresses this issue by qualitatively assess the fractional contribution of the vertical MSE advection to the zonal asymmetric pattern of the MSE tendency field, and how its contribution depends on the choice of the analysis domain, based on both observational and numerical simulation results. It is shown that the vertical MSE advection indeed plays a critical role in generating the zonal asymmetry of MSE tendency, accounting for 60% of the total MSE tendency field in observation and even more in aqua-planet simulations. It is indicated that the underestimated contribution from vertical MSE advection by some previous studies is attributed to the unphysical selection of analysis domain for the zonal asymmetric MSE tendency pattern.

1 Introduction

The Madden–Julian Oscillation (MJO) is the most prominent mode of intraseasonal variability in the tropics, characterized by an eastward propagating envelope of convective anomalies with a zonal wave number 1–3 spatial extent and 30–60-day time scale (e.g., Madden and Julian 1994; Zhang 2013; Li 2014). What physical processes dominate the slow eastward propagation of the MJO is a topic for debate. There are competing theories of the MJO, including the trio-interaction theory (Wang et al. 2016), the gravity-wave theory (Yang and Ingersoll 2013, 2014), the skeleton model (Majda and Stechmann 2009; Thual and Majda 2015) and the moisture mode theory (Sobel and Maloney 2013).

From the MJO "moisture mode" perspective, the eastward propagation of MJO convection is favored by processes moistening the region east of the convection center and drying the region west of it (e.g., Hsu and Li 2012; Sobel et al. 2014). Through conducting column-integrated moist static energy (MSE) budget analysis, it has been revealed that both the vertical MSE advection and the horizontal MSE advection could contribute to the east–west asymmetry of MSE tendency and thus leading to the MJO eastward propagation (Wang et al. 2017; Kim et al. 2014). The dominant processes for the vertical MSE advection to generate the zonal asymmetric MSE tendency is through the advection of background MSE by second baroclinic mode vertical velocity anomaly (Wang et al. 2017), which is clearly shown by the schematic diagram in Fig. 1. To the east of the MJO convection, a descending anomaly is in the upper level and an ascending anomaly is in the lower level; to the west, an ascending anomaly associated with stratiform-like heating is seen in the upper level while a descending anomaly is seen in the lower level. Given that the background MSE profile minimizes in the middle troposphere, such a distribution of vertical motion anomalies would induce a positive (negative) column-integrated MSE advection to the east (west). For the horizontal MSE advection, the advection of background MSE by low-level meridional wind anomalies plays a major role (Kim et al. 2014). To the east (west) of the

---

✉ Lu Wang
luwang@nuist.edu.cn

✉ Tim Li
timli@hawaii.edu

[1] Key Laboratory of Meteorological Disaster, Ministry of Education (KLME), Joint International Research Laboratory of Climate and Environmental Change (ILCEC), Collaborative Innovation Center on Forecast and Evaluation of Meteorological Disasters (CIC-FEMD), Nanjing University of Information Science and Technology, Nanjing, China

[2] Laboratory for Regional Oceanography and Numerical Modeling, Qingdao National Laboratory for Marine Science and Technology, Qingdao, China

[3] International Pacific Research Center, University of Hawai'i at Mānoa, Honolulu, USA

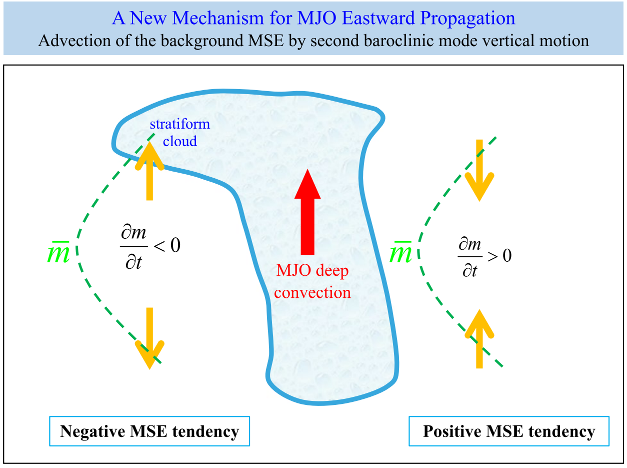

Fig. 1 Schematic diagram of the mechanism for vertical MSE advection favoring the MJO eastward propagation. The cloud describes a gross feature of an MJO that has a deep convective cloud-like structure over a broad region and a stratiform cloud-like structure in the rear in the upper troposphere. The green dashed curves denote climatological MSE profiles. The orange arrows to the east and to the west of the MJO convection region denote the second baroclinic mode vertical velocity anomalies. This figure is the same as Fig. 10 in Wang et al. (2017)

MJO convection, poleward (equatorward) meridional wind anomalies associated with cyclonic (anticyclonic) gyres appear. As the mean MSE (or moisture) maximizes near the equator, such a distribution of meridional wind anomalies would induce a positive (negative) MSE tendency to the east (west).

If the moisture mode theory for MJO is reasonable, a related question arises as what is the relative importance of the vertical and horizontal MSE advection to the MJO eastward propagation. Previous studies have widely conducted budget analyses of column-integrated MSE tendency to provide quantitative assessment of various processes in contributing to the MJO eastward propagation, yet no consensus has been achieved (e.g., Maloney 2009; Kiranmayi and Maloney 2011; Andersen and Kuang 2012; Wang et al. 2017; Jiang 2017). Some studies showed that the horizontal MSE advection plays a dominant role, while the contribution from the vertical MSE advection is negligible (e.g., Maloney 2009; Jiang 2017). But other studies presented that the vertical MSE advection is critical in the MJO eastward propagation, playing a comparable role with the zonal or meridional MSE advection (e.g., Hsu and Li 2012; Wang et al. 2017). Thus, an interesting question arises as what determines the differing assessments of the relative roles of vertical and horizontal MSE advections.

As most previous studies vary in considerable ways such as that they analyzed different datasets (reanalysis or model results) or they extracted the MJO based on different reference locations, it is impossible to compare those differing assessments directly. Most recently, two studies again highlighted a sharp contrast of the relative roles of vertical and horizontal MSE advection in contributing to the MJO eastward propagation. Jiang (2017) showed that the horizontal MSE advection is the leading term in generating the zonal asymmetric MSE tendency anomaly pattern [i.e., positive (negative) to the east (west)] which favors the MJO eastward propagation, while the contribution from the vertical MSE advection is negative. But Wang et al. (2017) showed that the vertical MSE advection could explain 80% of the total MSE tendency pattern. Interestingly, the two calculations were based on identical reanalysis data (ERA-interim) and the same MJO (located near 80° E), but only differed in analysis domains. Therefore, in this study we will re-investigate the relative roles of vertical and horizontal MSE advection in the MJO eastward propagation through a deep comparison of the effects of different analysis domains.

The rest of the paper is organized as below. The datasets and methods are described in Sect. 2; the comparison between the different assessments of vertical MSE advection is shown in Sect. 3; a discussion of the physical basis for analysis domain selection is presented in Sects. 4 and 5 gives the conclusion.

2 Data and method

2.1 Data

Here, we use observational daily precipitation data from Global Precipitation Climatology Project version 1.1 (GPCP; Huffman et al. 2001), and daily atmospheric reanalysis data from European Centre for Medium-Range Weather Forecasts (ECMWF) interim reanalysis (ERA-Interim; Dee et al. 2011) during boreal winter (November–April) from 1997 to 2008.

We also analyze the result from an atmospheric general circulation model simulation. The model used was developed at the Max Planck Institute for Meteorology with a horizontal resolution of T42 (i.e., ECHAM 4.6, Roeckner et al. 1996). This model is among one of the best models in simulating the MJO properties (Lin et al. 2006) and was previously used to study the northward propagation of the intraseasonal oscillation (ISO; Jiang et al. 2004) and real-case MJO prediction (Fu and Wang 2009). The experiment belongs to aqua-planet simulation, in which the model was driven by time-zonal invariant SST fields for 15 years, with orography removed and fixed equator-symmetric solar irradiance. The forcing SST profile peaks at the equator of 29 °C and decays with latitude, with a functional form of

$$SST(\phi) = \begin{cases} 29\left(1 - 0.25\sin^2\left(\frac{3\phi}{2}\right) - 0.75\sin^4\left(\frac{3\phi}{2}\right)\right)\,^{\circ}\mathrm{C}; & -\frac{\pi}{3} < \phi < \frac{\pi}{3}\,, \\ 0\,^{\circ}\mathrm{C}; \quad otherwise & \end{cases} \tag{1}$$

where ϕ represents latitude.

2.2 MSE budget analysis

A conventional budget analysis of column integrated MSE tendency on intraseasonal time scale is conducted in this study (Neelin and Held 1987). The MSE budget equation is written as

$$\langle \partial m/\partial t\rangle' = -\langle u\partial m/\partial x\rangle' - \langle v\partial m/\partial y\rangle' - \langle \omega\partial m/\partial p\rangle' + Q_t' + Q_r', \tag{2}$$

where angle brackets represent a mass-weighted vertical integral from the surface to 100-hPa level, p is pressure, u, v and ω are three-dimensional winds. Q_t represents the sum of surface latent heat flux and sensible heat flux, and Q_r represents the sum of column shortwave heating rate and longwave heating rate. A prime represents intraseasonal time scale.

2.3 Composite procedure of MJOs

Firstly, we filtered raw precipitation onto period of 20–80 days and eastward wavenumber 1–5 in the fashion of Wheeler and Kiladis (1999) to obtain MJO precipitation field. The filtered domain was chosen based on the zonal wavenumber-frequency power spectrum of observational precipitation during boreal winter (November–April) (see Fig. 2). Secondly, we calculated the standard deviation of the filtered precipitation (see Fig. 3) to identify the locations with the largest magnitude. Based on Fig. 3, two equally spaced reference boxes (10° × 10°) were selected, one at the eastern Indian Ocean (EIO, centered at 80° E, 5° S) and the other at the Maritime Continent (MC, centered at 140° E, 10° S) (marked by green boxes). Then, two MJO reference time series were constructed by box-averaged MJO rainfall. The MJO structure was composited by estimating linear regression coefficients using each MJO reference time series, which then were multiplied by a typical MJO rainfall anomaly (3 mm day^{-1}) to give the magnitudes of the field anomalies associated with an MJO event.

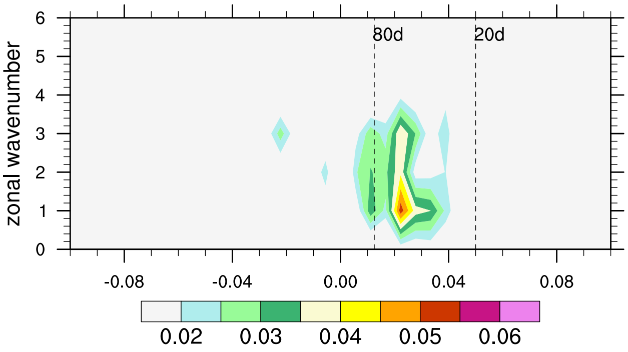

Fig. 2 Zonal wavenumber-frequency power spectrum of daily precipitation averaged over 10° S–10° N during boreal winter (November–April)

3 Results

3.1 Observational diagnosis

Figure 4a displays the horizontal distribution of column-integrated total MSE tendency anomaly (i.e., left-hand term of Eq. 2) relative to the EIO MJO. The green filled circle denotes the MJO reference center. It is clear that the MSE tendency anomaly shows an east–west asymmetric pattern [i.e., positive (negative) anomaly to the east (west)], consistent with the eastward propagation of the MJO rainfall maximum. Furthermore, the positive anomaly to the east has a larger zonal extension than the negative anomaly to the west, as the former corresponds to Kelvin wave response and the latter corresponds to Rossby wave response (Wang et al. 2017, 2018).

Next we examine the sensitivity of the relative roles of vertical and horizontal MSE advections to the analysis

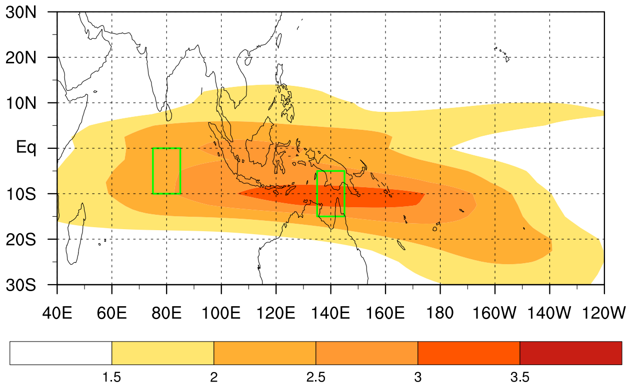

Fig. 3 Standard deviation of MJO filtered (i.e., period of 20–80 days and eastward wavenumbers 1–5) precipitation (mm day^{-1}) in boreal winter. The green rectangles represent the selected MJO reference boxes over the eastern Indian Ocean (EIO, 75°–85° E, 10° S–0° S) and the Maritime Continent (MC, 135°–145° E, 15° S–5° S). The precipitation data is derived from GPCP dataset

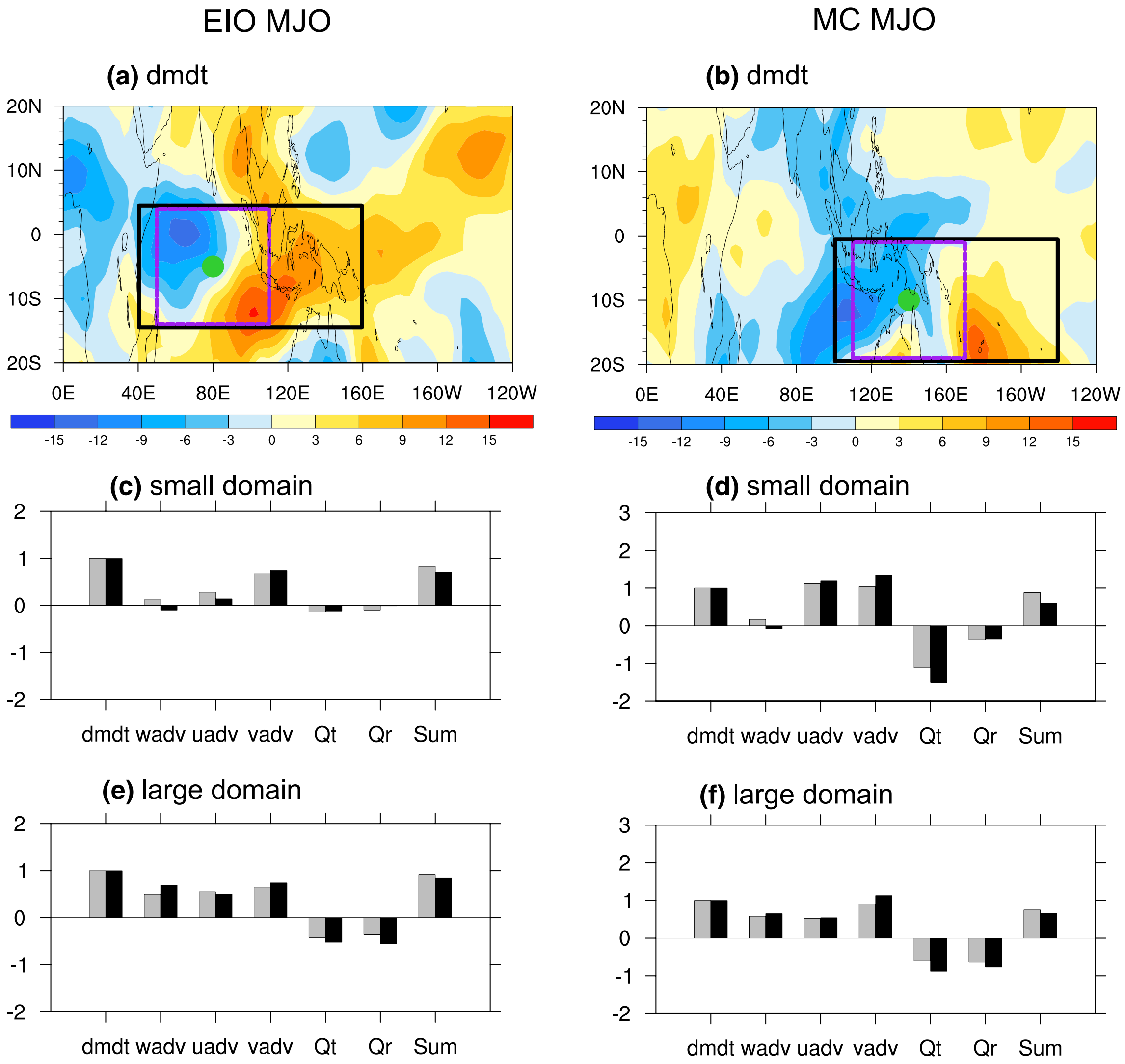

Fig. 4 (upper panels) Horizontal patterns of column-integrated total MSE tendency anomaly (W m^{-2}) associated with EIO MJO (**a**) and MC MJO (**b**). The green filled circles denote the MJO rainfall centers and the purple (black) boxes mark the small (large) analysis domains. (middle panels) Fractional contribution of each MSE budget component to the east–west asymmetric MSE tendency pattern over the small analysis domain for the EIO MJO (**c**) and MC MJO (**d**). The grey bars were calculated with spatial projection method, and the black bars were calculated through eastern-box average minus western-box average. The bars from left to right represent MSE tendency, vertical MSE advection, zonal MSE advection, meridional MSE advection, surface heat fluxes, atmospheric radiative term and sum of budget terms. (lower panels) Same as the middle panels, except for calculated over the large analysis domains for the EIO MJO (**e**) and MC MJO (**f**). The left (right) panels represent results from EIO (MC) MJO

domains. In Fig. 4a, the small purple box (50° E–110° E, 15° S–5° N) and the large black box (40° E–160° E, 15° S–5° N) denote two analysis domains for the EIO MJO; they only differ in zonal spans. The small one is identical to that adopted by Jiang (2017) while the large one is identical to that in Wang et al. (2017), except that they are shifted 5° southward compared to those in Jiang (2017) and Wang et al. (2017). This is due to the shift of the MJO reference center point in different studies [80° E, 5° S in this study vs. 80° E, 0° S in Jiang (2017) and Wang et al. (2017)].

Figure 4c, e show fractional contribution of each MSE budget quantity (i.e., right-hand terms of Eq. 2) to the east–west asymmetry of MSE tendency over the small and large analysis domains, respectively. Here we tried two calculations (grey bars vs. black bars). The grey bars were calculated by projecting each term onto the total MSE tendency anomaly pattern over an analysis domain in the form of

$$S_A = \frac{\iint \langle A\rangle\langle\partial_t m\rangle dxdy}{\iint \langle\partial_t m\rangle^2 dxdy}, \qquad (3)$$

where A denotes a particular process and $\iint dxdy$ denotes integral over the analysis domain. This projection method was originally proposed by Andersen and Kuang (2012) and was used to diagnose an MJO perturbation from an aqua-planet experiment, where the analysis domain was the whole tropical region. Studies further applied this method to diagnose the observed MJO perturbation and used limited domain near the MJO convection center for analysis (e.g., Arnold et al. 2015; Adames et al. 2016; Jiang 2017), considering that the observed MJOs exhibit much more complicated structure than the aqua-planet MJOs. It should be mentioned that as we focus on the asymmetric component between the east and the west parts of the MJO, the symmetric component near the MJO center with a zonal span of 20° in longitude was not included in the calculation. For instance, as the EIO MJO is centered at 80° E, the region of 70° E–90° E is excluded in the calculation over either the small or large domain. By definition, the projection coefficients could represent the fractional contributions from different processes. The black bars denote the difference of a term between an eastern box average and a western box average (east minus west); the zonal boundary of the eastern or western box is 10° away from the MJO center while the meridional boundaries are the same as the analysis domain. For the EIO MJO, the zonal ranges of eastern (western) box are 90° E–110° E (50° E–70° E) for the small analysis domain and 90° E–160° E (40° E–70° E) for the large analysis domain. After the east–west difference of each term is derived, then it is divided by the east–west difference of total MSE tendency anomaly in order to yield the fractional contribution.

As one can see, over the small analysis domain (Fig. 4c), the horizontal MSE advection plays a dominant role in generating the east–west asymmetric MSE tendency pattern, while the contribution from the vertical MSE advection is near-zero or even negative. However, the contribution from vertical MSE advection term is comparable to the zonal or meridional MSE advection term over the large analysis domain (Fig. 4e), with a fractional contribution of as high as 60%. The latter suggests that the vertical MSE advection term plays a substantial role in the MJO eastward propagation. Both calculations (grey and black bars) yield similar results, and the contrast related to the two analysis domains agree with the contrasting results between Jiang (2017) and Wang et al. (2017).

The right panels of Fig. 4 are the same as the left panels, except for the MC MJO. The purple and black boxes (i.e., 110° E–170° E, 20° S–0° N vs. 100° E–140° W, 20° S–0° N) marked in Fig. 4b represent analysis domains for the MC MJO. Note that the sizes of the two domains are identical to those in Fig. 4a, but the locations are adjusted according to the MJO reference point. The MSE budget results for the MC MJO agree with those for the EIO MJO. The contribution of vertical MSE advection to the zonal asymmetric MSE tendency pattern is near zero while that form the zonal or meridional MSE advection term is dominant over the small analysis domain (Fig. 4d). In contrast, the vertical MSE advection shows a comparable contribution as the zonal or meridional MSE advection term over the large analysis domain (Fig. 4f).

Then, why different analysis domains yield such conflicting assessments of the vertical MSE advection? To address this question, we examine the horizontal patterns of column-integrated vertical MSE advection term for both the EIO MJO and MC MJO (Fig. 5a, b). For the EIO MJO, the vertical MSE advection term shows a clear zonal asymmetry pattern with positive anomaly to the east and negative anomaly to the west (Fig. 5a), in particular if one removes the tendency over the main convective region (the purple box, or a region slightly smaller than the purple box). Such a zonal asymmetric pattern of vertical MSE advection indicates its contributing role in the MJO eastward propagation. But note that the positive anomaly of vertical MSE advection to the east extends far away from the MJO center and therefore only the large analysis domain (black box) could contain the complete zonal asymmetric pattern, while the small one (purple box) mainly contains the negative anomaly and reflects little of the zonal asymmetric pattern.

Furthermore, the horizontal pattern of column-integrated vertical MSE advection could be interpreted by the structure of MJO vertical velocity anomaly, because the vertical MSE advection is dominated by the advection of mean MSE profile by anomalous MJO vertical velocity (e.g., Wang et al. 2017; Arnold et al. 2015). Figure 5c displays the longitude-vertical cross section of MJO pressure velocity anomaly associated with the EIO MJO. An apparent zonal asymmetric pattern of vertical velocity anomaly relative to the MJO rainfall center is found: descending (ascending) anomalies in upper troposphere (boundary layer) appear to the east; ascending (descending) anomalies in upper troposphere (boundary layer) appear to the west. As the mean MSE minimizes in the mid-troposphere, the second baroclinic mode vertical velocity anomaly to the east and west of the MJO rainfall center could produce a zonally asymmetric vertical integral of vertical MSE advection. It is worth mentioning that the latter is mainly contributed by the upper-level component because the vertical velocity anomaly has a top-heavy structure. The zonal asymmetry of vertical velocity anomaly in upper troposphere is related to the presence of stratiform heating in the rear of the MJO convection (Wang et al. 2017). The purple and black boxes in Fig. 5c mark the small and large analysis domains, respectively. It is clear that the large analysis domain is able to cover the complete structure of the second baroclinic mode vertical velocity anomaly to the east and west of the MJO center while the small one

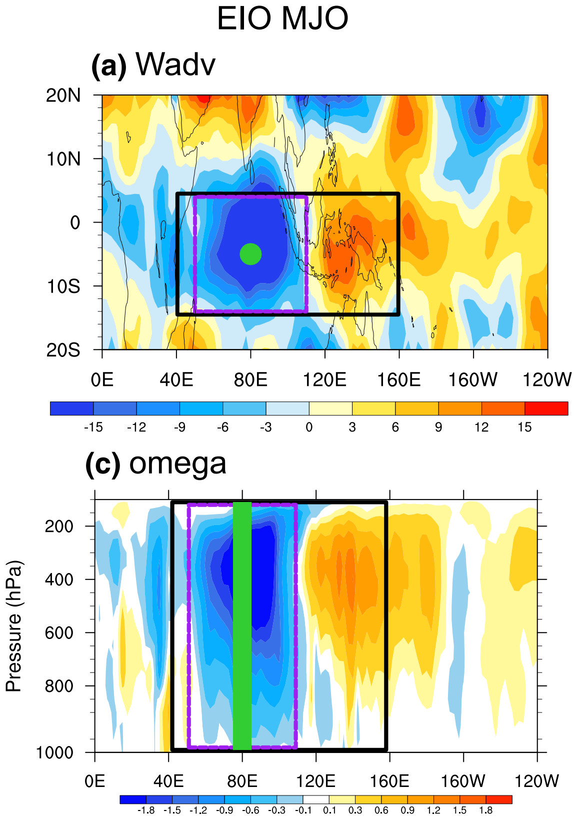

Fig. 5 (upper panels) Same as in Fig. 3a, b, except for column-integrated vertical MSE advective tendencies (W m^{-2}). (lower panels) Longitude-vertical cross section of pressure velocity anomaly (Pa s^{-1}) associated with EIO MJO (**c**) and MC MJO (**d**). The green filled circles or green bars denote the location of MJO rainfall centers. The purple (black) rectangles mark the small (large) analysis domains

does not. Therefore, the small analysis domain underestimates the zonal asymmetry of vertical MSE advection.

Compared to the case when the MJO convection is over the EIO, the vertical circulation pattern associated with the MC MJO is more complicated (Fig. 5b, d). The second baroclinic mode vertical structure is not well represented by the MC case. possibly due to fact that the MJO intensity is weakening over the MC and/or the effect of complicated topography land–sea distribution. To the east of the MJO rainfall center, the descending anomaly in upper troposphere is weaken, so the positive integral of vertical MSE advection to the east is weaken (see Fig. 5b). Generally speaking, the large analysis domain (black box) covers the critical structure of MC MJO vertical velocity anomaly as in the EIO MJO, so that it reflects large zonal asymmetry of vertical MSE advection, while the small one (purple box) does not.

The above comparisons reveal that the assessed relative roles of vertical and horizontal MSE advection in contributing to the MJO eastward propagation is very sensitive to the choice of analysis domain. If the analysis domain were too small, the zonal asymmetry of vertical MSE advection would be underestimated. Indeed, the vertical MSE advection is as important as the zonal or meridional MSE advection in generating the east-west asymmetric MSE tendency in observed MJOs.

3.2 Aqua-planet experiment diagnosis

Another way to verify the relative roles of vertical and horizontal MSE advection in contributing to the eastward propagation of MJO may be through diagnosing an aqua-planet MJO. A similar approach as done for compositing observed MJOs was used to composite the aqua-planet MJO. First, we obtain an MJO reference time series by filtering daily precipitation onto the MJO spectrum domain (i.e., 20–80 days and eastward wavenumbers 1–5) and averaging it over a small box of 160° E–170° E, 5° S–5° N. The reference box was chosen because the simulated intraseasonal rainfall variance maximizes at the equator and is zonally uniform (figure not shown); this is understandable with the presence of idealized SST forcing field. Then, all simulated fields were regressed against this MJO index to show MJO composite. Figure 6a displays the lagged time-longitude diagram of regressed precipitation anomaly averaged over 10° S–10° N. As is shown, this experiment simulates a prominent eastward propagating mode. Figure 6b displays the horizontal

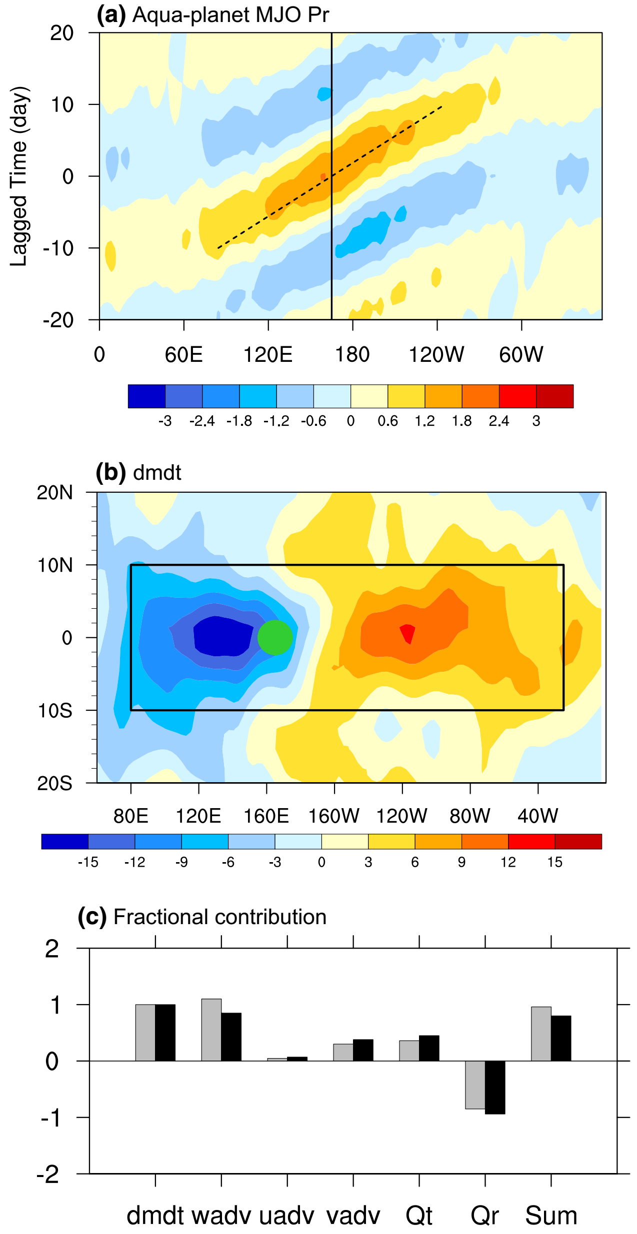

Fig. 6 **a** Lagged time-longitude diagram of precipitation anomaly (10° S–10° N average) regressed against MJO reference time series over 160°–170° E, 5° S–5° N. The result is obtained from Aqua-planet simulation. **b** Horizontal patterns of column-integrated total MSE tendency anomaly (W m^{-2}) at day 0. The green filled circle denotes the aqua-planet MJO rainfall center, and the black rectangle marks the analysis domain for aqua-planet MJO. **c** Same as in Fig. 1e, except for aqua-planet MJO

pattern of column-integrated total MSE tendency anomaly at day 0, when the MJO rainfall center is near 165° E. A prominent zonal asymmetric MSE tendency pattern relative to the MJO rainfall center is seen. Meanwhile, the positive MSE tendency anomaly to the east has a much larger zonal extension than that of the negative anomaly to the west, which is associated with Kelvin wave response to the east and Rossby wave response to the west. These features are all consistent with the observed MJOs, suggesting that the aqua-planet MJO could be a useful prototype for investigating the drivers for the MJO eastward propagation (Hsu et al. 2014). Therefore, in the following we present the MSE budget results for the aqua-planet MJO in the same fashion as in diagnosing the observed MJO.

Figure 6c displays the fractional contribution of each MSE tendency term to the zonal asymmetry of total MSE tendency pattern. Here, the analysis domain is chosen to cover the complete zonal asymmetric pattern of MSE tendency anomaly, similar as the large analysis domain for the observed MJOs. The black box in Fig. 6b denotes the analysis domain of 80° E–25° W, 10° S–10° N. The grey bars denote the result calculated by spatial projection method, while the black bars were calculated by the difference between an eastern box average and a western box average (east minus west). As in Sect. 3a, the symmetric part near the MJO center with a zonal span of 20° in longitude (i.e., 155° E–175° E) within the domain is excluded in the calculation, because we only focus on the zonal asymmetric component of MSE tendency anomaly. The zonal ranges of the eastern (western) box are 175° E–25° W (80° E–155° E). As seen from Fig. 6c, both calculations show that the vertical MSE advection term plays a dominant role in generating the zonal asymmetric MSE tendency, while the contribution from the horizontal MSE advection terms decrease compared to the observation, especially that the asymmetry of zonal advection component is near zero. As in the observation, the zonal asymmetry of the vertical MSE advective tendency in the aqua-planet MJO is related to the MJO vertical velocity anomaly of a second-baroclinic mode (figure not shown).

Then, why the zonal MSE advective tendency shows little asymmetry in the aqua-planet simulation? Figures 7a–c compare the horizontal patterns of the zonal MSE advective tendencies associated with the EIO MJO, MC MJO and the aqua-planet MJO. The black boxes indicate the eastern and western regions over the large analysis domains for calculating the east–west asymmetry of MSE tendency. The zonal advective tendencies for the EIO MJO present significant positive anomaly to the east and negative anomaly to the west and thus contribute significantly to the zonal asymmetry of MSE tendency (Fig. 7a). For the MC MJO, although a negative zonal MSE advective tendency appears at both sides, it is stronger at the west side than at the east side. As a result, the zonal MSE advection still contributes to the zonal-asymmetry of MSE tendency. The pattern of the observed zonal advective tendency is primarily contributed by the advection of mean MSE gradient by intraseasonal zonal wind. As the EIO MJO is west away of the mean moisture maximum near the Maritime Continent, its low-level easterly (westerly) wind anomaly to the east (west) generates positive (negative) zonal MSE advective tendency. As the MC MJO is near the the mean moisture maximum, its low-level easterly (westerly) wind anomaly to the east (west)

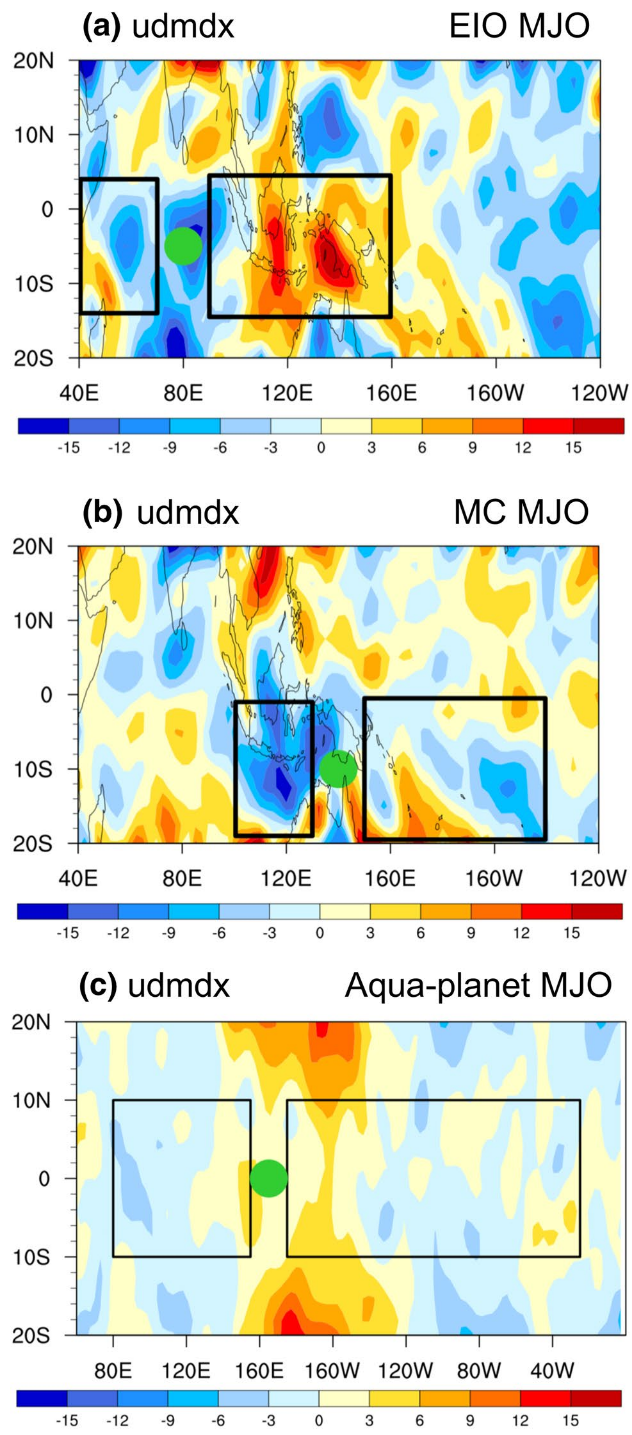

Fig. 7 Horizontal patterns of column-integrated zonal MSE advective tendencies (W m^{-2}) associated with EIO MJO (**a**), MC MJO (**b**) and aqua-planet MJO (**c**). The green filled circles denote the MJO rainfall centers, respectively. The black rectangles mark the eastern and western boxes used for calculating the east–west asymmetric MSE tendency over large analysis domains

both generate negative zonal MSE advective tendency. However, for the aqua-planet MJO, as the zonal gradient of mean moisture is zero, the advection of mean moisture by zonal wind anomaly is near zero, and therefore the zonal asymmetry of the zonal advection component disappears (Fig. 7c).

4 Discussion: selection of analysis domain

Section 3 has shown the sensitivity of the MSE budget result to the analysis domain. Here we discuss what is the physical basis for domain selection, and why the domain is zonal asymmetric relative to the MJO convective center.

As we know, the central point of the "moisture mode" theory is to connect MJO eastward propagation to zonal asymmetry of column integrated MSE tendency. Therefore, the domain selection should base on MJO-scale total MSE tendency pattern (e.g., Fig. 4a, b). As seen from Fig. 4a, b, the total MSE tendency pattern shows a clear east–west asymmetry, in particular if one removes the tendency over the main convective region (e.g., the purple box, or a region slightly smaller than the purple box).

Because the MJO circulation anomalies are critical in causing the zonally asymmetric MSE tendency pattern, an ideal analysis domain should cover the main MJO circulation. Gill (1982) showed that for a given limited region of forcing (i.e., diabatic heating), atmospheric response is far beyond the forcing region, due to atmospheric waves (e.g., eastward-propagating Kelvin waves and westward-propagating Rossby waves) that carry perturbation energy away from the forcing region. Given that Kelvin wave speed is three times faster than Rossby waves, for the same damping coefficient, Gill (1982) demonstrated that the length scale of the Kelvin wave response is three times as large as that of Rossby wave response. The vertical overturning circulation associated with low-level or upper-level divergence beyond the forcing region is a part of the wave response. This is the physical reason why one should use a zonally asymmetric domain (such as the black box shown in Fig. 4) to describe the main MJO circulation.

Let us carefully examine the zonal extent of the Kelvin and Rossby wave related circulation based on the observed MJO zonal wind and vertical velocity patterns. Figure 8a presents the zonal distribution of 700-hPa zonal wind anomaly (u700) averaged over a 20° latitude belt (15° S–5° N) associated with the MJO convection at EIO. To measure the zonal extent, the zonal wind anomaly is normalized by its maximum value. By choosing ± 0.3 as a criterion, one may find that the MJO easterly anomaly extends eastward to 180° E (indicated by the blue arrow) while the westerly anomaly extends westward to 45° E (indicated by the pink arrow). The ratio of the zonal extent of the easterly versus the westerly is approximately 3:1. The similar analysis may be conducted onto the vertical velocity anomaly at 400 hPa (ω400), where anomalous vertical motion is strongest (see Fig. 5c, d). As shown in Fig. 8b, the descending (ascending)

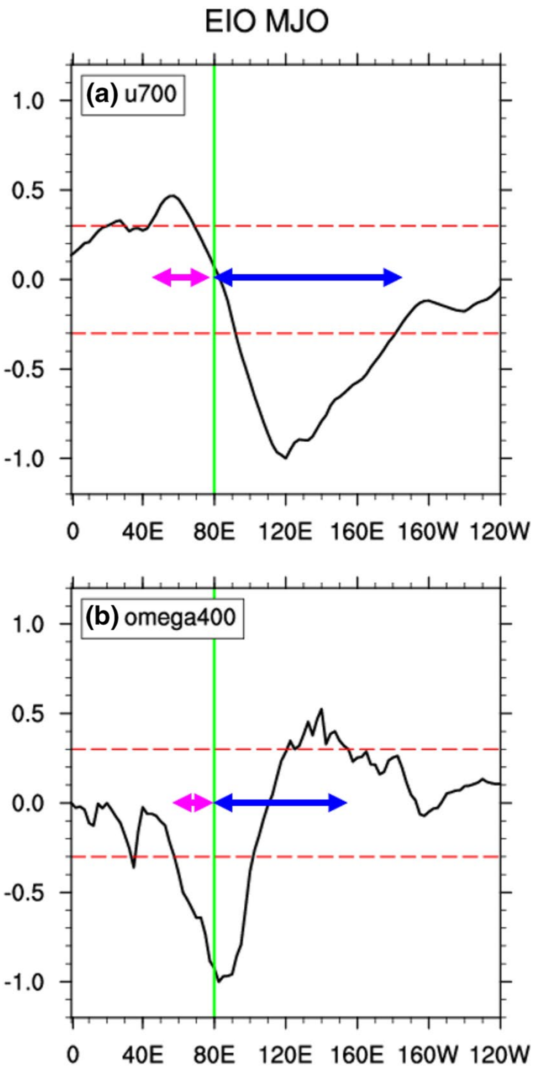

Fig. 8 Zonal distribution of 700-hPa zonal wind anomaly and 400-hPa pressure velocity anomaly averaged over 15° S–5° N associated with the EIO MJO convection. They were normalized by their corresponding maximum value. The red dashed lines mark the values of ±0.3, and the green lines denote the MJO convection center. The pink (blue) lines denote the zonal extension of the Rossby (Kelvin) wave component away from the MJO convection center, indicated by the value of ±0.3

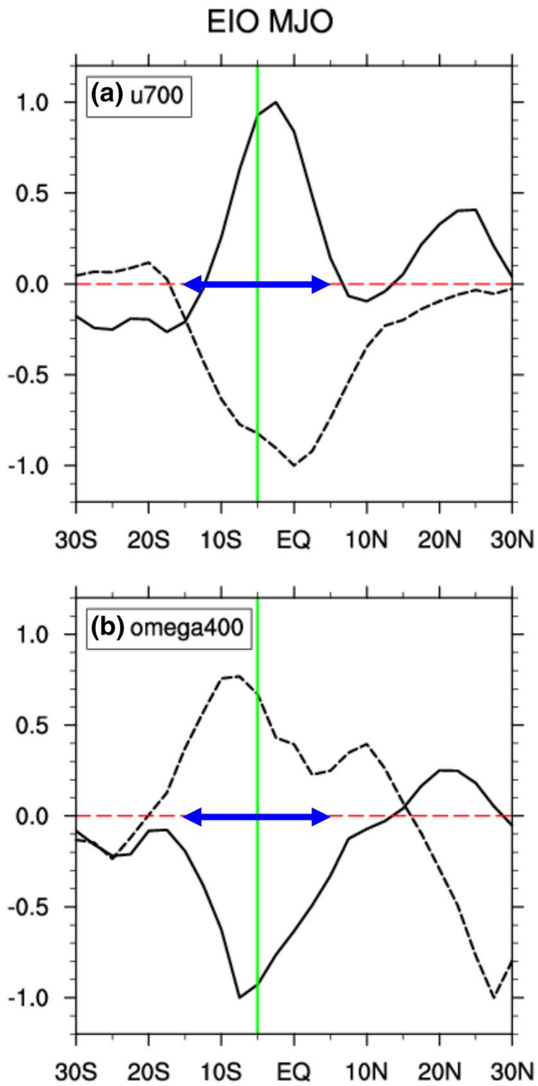

Fig. 9 Meridional profiles of 700-hPa zonal wind anomalies and 400-hPa pressure velocity anomalies to the east (dashed lines) and west (solid lines) of the EIO MJO center. The blue arrows indicate 20° meridional span

anomaly extends eastward (westward) to 152.5° E (57.5° E), and as a result, the ratio of the zonal extent of descending versus ascending anomaly is approximately 3:1. A similar result is obtained from the calculation of the MC case (figures not shown). Thus the observational results are consistent with the theoretical solution (Gill 1982). Therefore, to truly reflect the atmospheric Kelvin and Rossby wave effects, a larger, zonally asymmetric domain is needed.

Note that a smaller and symmetric domain such as the ones shown in the purple boxes in Fig. 4 represents primarily the symmetric part of the MSE tendency, not the zonally asymmetric part. It cannot reflect the true atmospheric Kelvin and Rossby wave components. For example, Fig. 5c shows that the most important zonal asymmetry arises from the region of 40° E–55° E and 110° E–160° E. At 40°–55° E, anomalous ascending motion appears in upper troposphere while anomalous descending motion appears in lower troposphere. An opposite vertical profile appears over 110° E–160° E. Such a second baroclinic mode vertical distribution favors a positive MSE tendency to the east and a negative MSE tendency to the west, promoting the eastward propagation (see Fig. 1, or Wang et al. 2017 for detailed discussion of this propagation mechanism). However, such an asymmetry is hardly seen in the purple domain.

Another issue is about meridional domain selection. One may use the same methodology to determine the meridional scale of the MJO circulation anomalies based on observed zonal wind and vertical motion anomalies. Figure 9a, b present the meridional profiles of u700 and ω400 to the east and west of the EIO MJO center, respectively. On average, the meridional length scale is about 20° in latitude, which is consistent with the analysis domains shown in Fig. 4. A similar result is obtained from the calculation of the MC case (figures not shown).

5 Conclusions

This study was aimed to re-assess the effect of vertical MSE advection to MJO eastward propagation, because previous studies have shown great uncertainty of its relative role. Some studies argued that the vertical advection is important to the MJO eastward propagation while other studies suggested that it has little effect. To address this issue, we calculated the fractional contribution of each MSE budget term to the east–west asymmetric pattern of total MSE tendency anomaly [i.e., positive (negative) anomaly to the east (west)], which has been assumed to favor the eastward movement of the MJO convection. To obtain more robust result, we examined observational MJOs over two locations, eastern Indian Ocean MJO and Maritime Continent MJO, as well as analyzed an aqua-planet experiment which simulates a prominent eastward-propagating MJO mode.

The observational diagnosis indicates that the vertical MSE advection accounts for about 60% of the zonal asymmetry of total MSE tendency anomaly, which is as important as the zonal or meridional MSE advection. This is in sharp contrast to some previous studies that showed the contribution from vertical advection term is near zero or even negative to the total MSE tendency anomaly while the horizontal advection plays a primary role. The substantial underestimation of role of the vertical MSE advection was attributed to unphysical selection of analysis domain for determining the zonal asymmetric MSE tendency pattern. It is argued that the analysis domain should be carefully designed to cover both the Kelvin wave and Rossby wave dynamic impacts by considering the zonal asymmetry of the MSE tendency pattern.

In the idealized aqua-planet simulation, the vertical MSE advection term shows an even greater contribution to the zonal asymmetry of the MSE tendency pattern. This is physically understood because with a zonally symmetric SST distribution, the mean moisture is zonal uniform, and as a result zonal MSE advection term is near zero and only meridional advection term contributes to the horizontal MSE advection. It should be mentioned that the idealized aqua-planet simulation result is sensitive to the forcing field of SST distribution pattern as revealed by Wang et al. (2018). If the curve of the meridional profile of zonally symmetric SST distribution near the equator were set to be smaller, the simulated mean moisture would not peak at the equator as the observation but show maximums to the north and to the south of the equator, respectively. In that case, the meridional advection of mean MSE by MJO meridional wind anomalies would not contribute to the eastward propagation of the MJO convection.

Acknowledgements This work was supported by NSFC Grants 41975108/41705059/41875069, NSF Grant AGS-1643297, NOAA Grant NA18OAR4310298, NSFC-Shandong Joint Fund for Marine Science Research Centers (U1606405) and the Startup Foundation for Introducing Talent of NUIST. This is SOEST contribution number 1234, IPRC contribution number 1234, and ESMC contribution 299.

References

Adames ÁF, Wallace JM, Monteiro JM (2016) Seasonality of the structure and propagation characteristics of the MJO. J Atmos Sci 73:3511–3526. https://doi.org/10.1175/JAS-D-15-0232.1

Andersen JA, Kuang Z (2012) Moist static energy budget of MJO-like disturbances in the atmosphere of a zonally symmetric aquaplanet. J Clim 25:2782–2804. https://doi.org/10.1175/jcli-d-11-00168.1

Arnold NP, Branson M, Kuang Z et al (2015) MJO intensification with warming in the superparameterized CESM. J Clim 28:2706–2724. https://doi.org/10.1175/JCLI-D-14-00494.1

Dee DP, Uppala SM, Simmons AJ et al (2011) The ERA-Interim reanalysis: configuration and performance of the data assimilation system. Q J R Meteorol Soc 137:553–597. https://doi.org/10.1002/qj.828

Fu X, Wang B (2009) Critical Roles of the stratiform rainfall in sustaining the madden–julian sscillation: GCM experiments. J Clim 22:3939–3959. https://doi.org/10.1175/2009JCLI2610.1

Gill AE (1982) Atmosphere-ocean dynamics, international geophysics series. Academic Press, Waltham, pp 599–602

Hsu P, Li T (2012) Role of the boundary layer moisture asymmetry in causing the eastward propagation of the Madden–Julian oscillation. J Clim 25:4914–4931. https://doi.org/10.1175/jcli-d-11-00310.1

Hsu P-C, Li T, Murakami H (2014) Moisture asymmetry and MJO eastward propagation in an aquaplanet general circulation model. J Clim 27:8747–8760. https://doi.org/10.1175/jcli-d-14-00148.1

Huffman GJ, Adler RF, Morrissey MM et al (2001) Global precipitation at one-degree daily resolution from multisatellite observations. J Hydrometeorol 2:36–50. https://doi.org/10.1175/1525-7541(2001)002<0036:gpaodd>2.0.co;2

Jiang X (2017) Key processes for the eastward propagation of the Madden–Julian oscillation based on multimodel simulations. J Geophys Res Atmos 122:755–770. https://doi.org/10.1002/2016jd025955

Jiang X, Li T, Wang B (2004) Structures and mechanisms of the northward propagating boreal summer intraseasonal oscillation. J Clim 17:1022–1039. https://doi.org/10.1175/1520-0442(2004)017<1022:SAMOTN>2.0.CO;2

Kim D, Kug J-S, Sobel AH (2014) Propagating versus nonpropagating Madden–Julian oscillation events. J Clim 27:111–125. https://doi.org/10.1175/jcli-d-13-00084.1

Kiranmayi L, Maloney ED (2011) Intraseasonal moist static energy budget in reanalysis data. J Geophys Res Atmos 116:D21117. https://doi.org/10.1029/2011jd016031

Li T (2014) Recent advance in understanding the dynamics of the Madden–Julian oscillation. J Meteorol Res 28:1–33. https://doi.org/10.1007/s13351-014-3087-6

Lin J-L, Kiladis GN, Mapes BE et al (2006) Tropical intraseasonal variability in 14 IPCC AR4 climate models. Part I: convective signals. J Clim 19:2665–2690. https://doi.org/10.1175/jcli3735.1

Madden RA, Julian PR (1994) Observations of the 40–50-day tropical oscillation: a review. Mon Weather Rev 122:814–837

Majda AJ, Stechmann SN (2009) The skeleton of tropical intraseasonal oscillations. Proc Natl Acad Sci 106:8417–8422. https://doi.org/10.1073/pnas.0903367106

Maloney ED (2009) The moist static energy budget of a composite tropical intraseasonal oscillation in a climate model. J Clim 22:711–729. https://doi.org/10.1175/2008JCLI2542.1

Neelin JD, Held IM (1987) Modeling tropical convergence based on the moist static energy budget. Mon Weather Rev 115:3–12. https://doi.org/10.1175/1520-0493(1987)115<0003:mtcbot>2.0.co;2

Roeckner E, Arpe L, Bengtsson L et al (1996) The atmospheric general circulation model ECHAM4: model description and simulation of present-day climate. Max-Planck-Institut für Meteorologie, Hamburg

Sobel A, Maloney E (2013) Moisture modes and the eastward propagation of the MJO. J Atmos Sci 70:187–192. https://doi.org/10.1175/JAS-D-12-0189.1

Sobel A, Wang S, Kim D (2014) Moist static energy budget of the MJO during DYNAMO. J Atmos Sci 71:4276–4291. https://doi.org/10.1175/jas-d-14-0052.1

Thual S, Majda AJ (2015) A suite of skeleton models for the MJO with refined vertical structure. Math Clim Weather Forecast 1:89. https://doi.org/10.1515/mcwf-2015-0004

Wang B, Liu F, Chen G (2016) A trio-interaction theory for Madden–Julian oscillation. Geosci Lett 3:34. https://doi.org/10.1186/s40562-016-0066-z

Wang L, Li T, Maloney E, Wang B (2017) Fundamental causes of propagating and non-propagating MJOs in MJOTF/GASS models. J Clim 30:3743–3769. https://doi.org/10.1175/JCLI-D-16-0765.1

Wang L, Li T, Nasuno T (2018) Impact of Rossby and Kelvin wave components on MJO eastward propagation. J Clim 31:6913–6931. https://doi.org/10.1175/JCLI-D-17-0749.1

Wheeler M, Kiladis GN (1999) Convectively coupled equatorial waves: analysis of clouds and temperature in the wavenumber–frequency domain. J Atmos Sci 56:374–399. https://doi.org/10.1175/1520-0469(1999)056<0374:ccewao>2.0.co;2

Yang D, Ingersoll AP (2013) Triggered convection, gravity waves, and the MJO: a shallow-water model. J Atmos Sci 70:2476–2486. https://doi.org/10.1175/JAS-D-12-0255.1

Yang D, Ingersoll AP (2014) A theory of the MJO horizontal scale. Geophys Res Lett 41:89. https://doi.org/10.1002/2013gl058542

Zhang C (2013) Madden–Julian oscillation: bridging weather and climate. Bull Am Meteorol Soc 94:1849. https://doi.org/10.1175/bams-d-12-00026.1